

Contrasting the chemical evolution of the Milky Way and Andromeda galaxies

Agostino Renda^{1*}, Daisuke Kawata^{1*}, Yeshe Fenner^{1*}, Brad K. Gibson^{1*}

¹Centre for Astrophysics & Supercomputing, Swinburne University, Hawthorn, Victoria, 3122, Australia

Accepted. Received; in original form

ABSTRACT

The chemical evolution history of a galaxy hides clues about how it formed and has been changing through time. We have studied the chemical evolution history of the Milky Way (MW) and Andromeda (M31) to find which are common features in the chemical evolution of disc galaxies as well as which are galaxy-dependent. We use a semi-analytic multi-zone chemical evolution model. Such models have succeeded in explaining the mean trends of the observed chemical properties in these two Local Group spiral galaxies with similar mass and morphology. Our results suggest that while the evolution of the MW and M31 shares general similarities, differences in the formation history are required to explain the observations in detail. In particular, we found that the observed higher metallicity in the M31 halo can be explained by either a) a higher halo star formation efficiency or b) a larger reservoir of infalling halo gas with a longer halo formation phase. These two different pictures would lead to a) a higher [O/Fe] at low metallicities or b) younger stellar populations in the M31 halo, respectively. Both pictures result in a more massive stellar halo in M31, which suggests a possible correlation between the halo metallicity and its stellar mass.

Key words: galaxies: chemical evolution – galaxies: halos – galaxies: formation – galaxies: evolution

1 INTRODUCTION

The chemical properties of galaxies hide clues about their formation and evolution. Semi-analytic chemical evolution models (Talbot & Arnett 1971; Tinsley 1980) have succeeded in explaining the mean trends of galactic systems by numerically solving a set of equations governing the simplified evolution of the chemical elements as they cycle through gas and stars. One strength of these models is that they typically have the fewest number of free parameters, making convergence to a smaller set of solutions more likely.

Strong constraints can be placed on chemical evolution models only by contrasting them against a comprehensive set of observed properties. Since the most detailed observational data are generally available for the Milky Way (e.g. Freeman & Bland-Hawthorn 2002), successful agreement between model predictions and these observed properties has been obtained by several studies in the past, which help us to understand the formation history of the Milky Way (MW). Some models have focused on the evolution of the chemical abundances both in the solar neighbourhood and in the whole disc, adopting a frame-

work in which the MW has been built-up inside-out by means of a single accretion event (e.g. Matteucci & François 1989; Pagel & Tautvaišienė 1995). Others have used an early infall of gas to explain the thick disc formation, followed by a slower infall to form the thin disc (e.g. Chiappini, Matteucci & Gratton 1997). Several studies have paid particular attention to the chemical evolution of a larger range of elements (e.g. Timmes, Woosley & Weaver 1995; Goswami & Prantzos 2000; Alibés, Labay & Canal 2001) or focused on the features of the Metallicity Distribution Function (MDF) in the solar neighbourhood (e.g. Fenner & Gibson 2003). However, an implicit assumption remains unanswered: *is the MW a typical spiral?*

Andromeda (M31) is the closest spiral to our MW (e.g. van den Bergh 2003). Previous theoretical studies of the chemical evolution of M31 have been done by Diaz & Tosi (1984) and Mollá, Ferrini & Diaz (1996), both emphasising the evolution of the M31 disc. They concluded that M31 has a formation history and chemical evolution similar to that of the MW. More recently, however, there has been considerable observational progress in the study of both galaxies. A striking difference between M31 and the MW is that the

* E-mail: arenda,dkawata,yfenner,bgibson@astro.swin.edu.au

metallicity of the M31 halo ($\langle[\text{Fe}/\text{H}]\rangle \approx -0.5$)¹ is significantly higher than its MW analogue ($\langle[\text{Fe}/\text{H}]\rangle \approx -1.8$, e.g. Ryan & Norris 1991), as revealed by many recent studies (e.g. Holland, Fahlman & Richer 1996; Durrell, Harris, & Pritchett 2001; Sarajedini & van Duyn 2001; Ferguson & Johnson 2001; Reitzel & Guhathakurta 2002; Ferguson et al. 2002; Worthey & España 2003; Bellazzini et al. 2003; Brown et al. 2003; Reitzel et al. 2004; Rich et al. 2004).

It is therefore timely to attempt the construction of a chemical evolution model for both the MW and M31, using the same framework. Such an attempt may be helpful in highlighting the common features in the chemical evolution of spiral galaxies (at least in these two spirals) and those which remain galaxy-dependent.

In Section 2 we describe our multi-zone chemical evolution model, and in Section 3 we present the results of our MW model. In Section 4 we show the results for M31. Finally, our results are discussed in Section 5.

2 THE MODEL

In this study we use a semi-analytic multi-zone chemical evolution model for a spiral galaxy. This model is based on **GETool** (Fenner & Gibson 2003; Gibson et al. 2003). We follow the chemical evolution of the halo and disc of M31 and the MW under the assumption that both galaxies are formed from two phases of gas infall. The first infall episode corresponds to the halo build-up, and the second to the inside-out formation of the disc. Similar formalisms have been successful in modeling the chemical evolution of the solar neighbourhood (e.g. Chiappini, Matteucci & Gratton 1997; Chang et al. 1999; Alibés, Labay & Canal 2001). We assume that halo stars were born in a burst induced by the collapse of a single proto-galactic cloud (Eggen, Lynden-Bell & Sandage 1962) or by the multiple merger of building-blocks (Searle & Zinn 1978; Bekki & Chiba 2001; Brook et al. 2003). The disc is assumed to be built-up inside-out by the smooth accretion of gas on a longer timescale. Observations of HI High Velocity Clouds (HVCs) that appear to be currently falling onto the MW (e.g. Putman et al. 2003 and references therein) may provide evidence for such gas infall. Recently, HVCs have also been detected in the M31 neighbourhood, though their interpretation as infalling clouds is debated (Thilker et al. 2004).

We monitor the face-on projected properties of the halo and disc components. While this geometrical simplification is suitable for approximating the flat disc, it is less appropriate for the halo, whose shape is roughly spherical rather than disc-like. However, we consider this choice acceptable in a simplified model of the chemical evolution of a spiral galaxy. We follow the chemical evolution of several independent rings, 2 kpc wide, out to a galactocentric radius $R = 10R_d$, where R_d is the disc scale-length. We also ignore the bulge component, because we are interested in the relatively outer region ($R > 4$ kpc). Each ring is a single zone onto which gas falls, without exchange of matter between

the rings. We trace the chemical evolution of each zone individually. In our model, we assume that the age of the galaxy is $t_{now} = 13$ Gyr. The basic equations (e.g. Tinsley 1980), in a zone at a radius R , for the evolution of the gas surface density $\Sigma_{g,i}(R, t)$ of an element i are written as follows:

$$\begin{aligned} \dot{\Sigma}_{g,i}(R, t) = & \\ - \psi(R, t)X_i(R, t) & + \int_{M_{min}}^{M_{Bmin}} \psi(R, t - \tau_m) \\ \times Y_i(m, Z_{t-\tau_m}) \frac{\varphi(m)}{m} dm & + k \int_{M_{Bmin}}^{M_{Bmax}} \frac{\varphi(M_B)}{M_B} \\ \times \int_{\mu_{min}}^{0.5} f(\mu) \psi(R, t - \tau_{m_2}) Y_i(M_B, Z_{t-\tau_{m_2}}) d\mu dM_B & \\ + (1 - k) \int_{M_{Bmin}}^{M_{Bmax}} \psi(R, t - \tau_m) Y_i(m, Z_{t-\tau_m}) & \\ \times \frac{\varphi(m)}{m} dm + \int_{M_{Bmax}}^{M_{max}} \psi(R, t - \tau_m) Y_i(m, Z_{t-\tau_m}) & \\ \times \frac{\varphi(m)}{m} dm + X_{i,halo}(t) h(R) e^{\frac{-t}{\tau_h}} & \\ + X_{i,disc}(t) d(R) e^{\frac{-(t-t_{delay})}{\tau_d(R)}}. & \end{aligned} \quad (1)$$

Here $X_i(R, t) = \frac{\Sigma_{g,i}(R, t)}{\Sigma_g(R, t)}$ is the mass fraction for the element i ; $\psi(R, t)$ is the star formation rate (SFR); $\varphi(m)$ is the Initial Mass Function (IMF) with the mass range $M_{min} - M_{max}$; τ_m is the lifetime of a star with mass m ; $Y_i(m, Z_{t-\tau_m})$ is the stellar yield of the element from a star of mass m , age τ_m and metallicity $Z_{t-\tau_m}$. The first term describes the depletion of the element i which is locked-up in newly formed stars. The second and the fourth terms show the contribution of mass loss from low and intermediate mass stars. The third term describes the contribution from Type Ia SNe (SNeIa). The contribution from SNeIa is calculated as suggested in Greggio & Renzini (1983), where k , M_{Bmin} , M_{Bmax} , μ_{min} , μ , $f(\mu)$, τ_{m_2} are defined. The fifth term shows the contribution from Type II SNe (SNeII). The sixth and the seventh terms represent the infalling halo and disc gas, respectively.

The Kroupa, Tout & Gilmore (1993) IMF is used here. We have chosen a lower mass limit of $M_{min} = 0.08 M_\odot$ and imposed an upper mass limit of $M_{max} = 60 M_\odot$ in order to avoid the overproduction of oxygen and recover the observed trend of $[\text{O}/\text{Fe}]$ at low metallicity at the solar neighbourhood in the MW. Such IMF upper mass limit is currently loosely constrained by stellar formation and evolution models. Yet, these stellar models, and the yields they provide, are one of the most important features in galactic chemical evolution, although questions remain concerning the precise composition of stellar ejecta, due to the uncertain role played by processes including mass loss, rotation, fall-back, and the location of the mass cut, which separates the remnant from the ejected material in SNe. The SNeII yields are from Woosley & Weaver (1995). We have halved the iron yields shown in Woosley & Weaver (1995), as suggested by Timmes et al. (1995). The SNeIa yields are from Iwamoto et al. (1999). The metallicity-dependent yields of Renzini & Voli (1981) have been used for stars in the range 1 - 8 M_\odot . The lifetimes of stars as a function of mass and metallicity have been taken from Schaller et al. (1992).

¹ Hereafter $[X/\text{Fe}] = \log_{10}(X/\text{Fe}) - \log_{10}(X/\text{Fe})_\odot$.

Table 1. The parameters for the MW and M31 models.

	α	$\Sigma_{t,h}(R_\odot, t_{now})$ ($M_\odot \text{ pc}^{-2}$)	R_d (kpc)	$\Sigma_{t,d}(R_\odot, t_{now})$ ($M_\odot \text{ pc}^{-2}$)	τ_h (Gyr)	t_{delay} (Gyr)	a_d (Gyr)	b_d	ν_h	ν_d
MW	2	6	3.0	48	0.1	1.0	2.0	1.25	0.125	0.03
M31a	2	6	5.5	46	0.1	1.0	2.0	1.25	0.125	0.03
M31b	2	6	5.5	46	0.1	1.0	0.7	0.50	12.5	0.08
M31c	2	57	5.5	46	0.5	6.0	0.1	0.10	0.125	0.08

2.1 Infall

The infall rate during the halo and disc phases is simply assumed to decline exponentially, as seen by the adopted sixth and seventh terms in equation (1). The evolution of the total² surface mass density, $\Sigma_t(R, t)$, is described by:

$$\frac{d\Sigma_t(R, t)}{dt} = h(R)e^{\frac{-t}{\tau_h}} + d(R)e^{\frac{-(t-t_{delay})}{\tau_d(R)}}. \quad (2)$$

Here, the first term describes the infall rate in the halo phase. The infall time-scale in the halo phase, τ_h , is assumed to be independent of radius, for simplicity. The infall of disc gas starts with a delay of t_{delay} , as seen in the second term. The time-scale of the disc infall depends on radius as follows:

$$\tau_d(R) = a_d + b_d \frac{R}{\text{kpc}} \text{Gyr}. \quad (3)$$

The values for the constants a_d and b_d are free parameters. The infall coefficients $h(R)$ and $d(R)$ are chosen in order to reproduce the present-day total surface density in the disc, $\Sigma_{t,d}(R, t_{now})$, and halo, $\Sigma_{t,h}(R, t_{now})$, respectively, as follows (e.g. Timmes et al. 1995):

$$h(R) = \Sigma_{t,h}(R, t_{now}) \times \left\{ \tau_h \left[1 - \exp\left(\frac{-t_{now}}{\tau_h}\right) \right] \right\}^{-1}; \quad (4)$$

$$d(R) = \Sigma_{t,d}(R, t_{now}) \times \left\{ \tau_d(R) \left[1 - \exp\left(-\frac{t_{now} - t_{delay}}{\tau_d(R)}\right) \right] \right\}^{-1}. \quad (5)$$

The infalling halo gas has been assumed to be of primordial composition. On the other hand, it is unlikely that the accreting gas has primordial abundance at a later epoch, since even low density inter-galactic medium, such as the Lyman α forest, has a significant amount of metals (e.g. Cowie & Songalia 1998), and it is known that the HVCs in the MW, which may be infalling gas clouds, have metallicities between 0.1 and 0.3 Z_\odot (Sembach et al. 2002). Therefore, we assume that the gas accreting onto the disc is pre-enriched. The level of pre-enrichment can be loosely constrained from the observed metallicity of Galactic HVCs. We simply assume that the metallicity of the infalling disc material is $Z_{infall}(R, t) = Z(R, t)$ if $Z(R, t) < Z_{infall,max} = 0.3 Z_\odot$, where $Z(R, t)$ is the metallicity of the gas at the radius R and the time t , otherwise $Z_{infall}(R, t) = Z_{infall,max} = 0.3 Z_\odot$. The abundance pattern of the infalling disc gas is further unknown parameter. Following the

above simple assumption, we set the infalling disc gas, at a given galactocentric radius R and time t , to have the same abundance pattern as the ISM at R and t . This guarantees the smooth evolution of the gas abundance and of the abundance patterns in each radial bin.

2.2 Disc and halo surface density profiles

We adopt the following exponential profile for the present-day total surface density of the disc component:

$$\Sigma_{t,d}(R, t_{now}) = \Sigma_{t,d}(R_\odot, t_{now}) e^{-(R-R_\odot)/R_d}. \quad (6)$$

Here $R_\odot = 8$ kpc, which is the galactocentric distance of the Sun within the MW. The same definition of $R_\odot = 8$ kpc is applied to the M31 models.

The surface density profiles of the MW and M31 disc are different. We have chosen a scale-length of $R_d = 3.0$ kpc for the MW (e.g. Robin, Creze & Mohan 1992; Ruphy et al. 1996; Freudenreich 1998) and $R_d = 5.5$ kpc for M31 (Walterbos & Kennicutt 1988). For the MW, we assume $\Sigma_{t,d}(R_\odot, t_{now}) = 48 M_\odot \text{ pc}^{-2}$ (Kuijken & Gilmore 1991). We adopt $\Sigma_{t,d}(R_\odot, t_{now}) = 46 M_\odot \text{ pc}^{-2}$ in M31, such that the mass of the M31 disc is similar to that of the MW disc ($\approx 10^{11} M_\odot$ as in Freeman 1999).

We adopt a modified Hubble law for the present-day total surface density profile of the halo (Binney & Tremaine 1987):

$$\Sigma_{t,h}(R, t_{now}) = \frac{\Sigma_{t,h_0}}{1 + (R/R_\odot)^\alpha}. \quad (7)$$

Here we set $\alpha = 2$. This corresponds to a volume halo density profile:

$$\rho_{t,h}(r, t_{now}) = \frac{\rho_{t,h_0}}{\left[1 + \left(\frac{r}{R_\odot}\right)^2 \right]^{3/2}}, \quad (8)$$

with $\rho_{t,h_0} = 2^{3/2} \rho_{t,h}(R_\odot, t_{now})$ and $\Sigma_{t,h_0} = 2R_\odot \rho_{t,h_0}$. For the MW, we assume $\Sigma_{t,h}(R_\odot, t_{now}) = 6 M_\odot \text{ pc}^{-2}$ which yields a present-day stellar surface density at R_\odot of $\Sigma_{\star,h}(R_\odot, t_{now}) = 1.3 M_\odot \text{ pc}^{-2}$ for our model (see Section 3), which is consistent with the observed halo stellar density at the solar radius $\rho_{\star,h}(R_\odot, t_{now}) = 5.7 \times 10^4 M_\odot \text{ kpc}^{-3}$ as estimated by Preston, Shectman & Beers (1991).

The assumption of $\alpha = 2$, which implies $\rho_{\star,h} \propto r^{-3}$, agrees with a recent analysis (Zibetti, White & Brinkmann 2003) of the halo emission for a sample of ≈ 1000 edge-on disc galaxies within the Sloan Digital Sky Survey (SDSS). This result is similar to the density profile $\propto r^{-3.5}$ which has been suggested for the MW stellar halo (Chiba & Beers 2000; Chiba & Beers 2001; Sakamoto, Chiba & Beers 2003).

² Hereafter, by ‘‘total’’ density we mean the sum of the stellar and gas densities.

2.3 Star Formation Rate

We assume that the halo star formation (SF) happens on a short time-scale because of a rapid infall event associated with the collapse of a single massive proto-galactic cloud (Eggen et al. 1962) or multiple mergers of building-blocks (Searle & Zinn 1978). The disc SF is assumed to be a more quiescent phenomenon, and likely to be driven by the spiral arms (e.g. Wyse & Silk 1989). Therefore, we adopt a different SF law for each component.

The adopted halo SFR is described as:

$$\psi_h(R, t) = \nu_h \left(\frac{\Sigma_g(R, t)}{1 M_\odot \text{ pc}^{-2}} \right)^{1.5} M_\odot \text{ Gyr}^{-1} \text{ pc}^{-2}, \quad (9)$$

where ν_h is the star formation efficiency (SFE) in the halo. Therefore, the halo SFR follows a Schmidt law with exponent 1.5 (e.g. Kennicutt 1998). The adopted halo SFE is $\nu_h = 0.125$, which is approximately half of the value ($\nu_h = 0.25 \pm 0.07$) suggested by Kennicutt (1998) and is chosen to give the best fit to the observed halo MDF at the solar neighbourhood (see Section 3). Stars born before t_{delay} , when the disc phase starts (Section 2.1), are hereafter labelled as ‘‘halo stars’’.

The adopted disc SFR is written as:

$$\psi_d(R, t) = \nu_d \Sigma_g(R, t)^2 \frac{R_\odot}{R} M_\odot \text{ Gyr}^{-1} \text{ pc}^{-2}, \quad (10)$$

where ν_d is the SFE in the disc. This formulation (Wyse & Silk 1989) reflects the assumption that SF in the disc is triggered by the compression of the ISM by spiral arms. The efficiency factor ν_d is a free parameter. We have found that ν_d affects both the present-day gas fraction and the disc MDF. The value $\nu_d = 0.03$ is used in our MW model to reproduce the observed gas density profile of the MW disc and the observed MDF at the solar neighbourhood.

3 THE MILKY WAY MODEL

Using the multi-zone model described in the previous section, we construct a model which most closely reproduces the known observational properties of the MW. The adopted parameters are summarised in Table 1 (MW model).

Fig. 1a compares the model MDF at the solar neighbourhood with the observed MDF of K dwarfs (Kotoneva et al. 2002). Here we have assumed a K dwarf mass range of 0.8 - 1.4 M_\odot and convolved the MDF of the model with a Gaussian error function with $\sigma = 0.15$ dex, consistent with the known empirical uncertainties of the observational data. There is good agreement between the model and the data. In Fig. 1b, the predicted halo MDF at the solar radius is shown. Our MDF includes all stars still on the main-sequence at the present-time. The MDF has been convolved with a Gaussian error function with $\sigma = 0.25$ dex (e.g. Asplund 2003). Our model is in agreement with the observed halo MDF at the solar neighbourhood (Ryan & Norris 1991). The evolution of $[\text{O}/\text{Fe}]$ as a function of $[\text{Fe}/\text{H}]$ for the gas component in the solar neighbourhood is shown in Fig. 1c. The model result is consistent with the trend of $[\text{O}/\text{Fe}]$ and $[\text{Fe}/\text{H}]$ observed in local stars. Fig. 1d displays the predicted SF history at the solar neighbourhood. The SF history has been estimated by several authors (e.g. Bertelli & Nasi 2001; Hernandez et al. 2000).

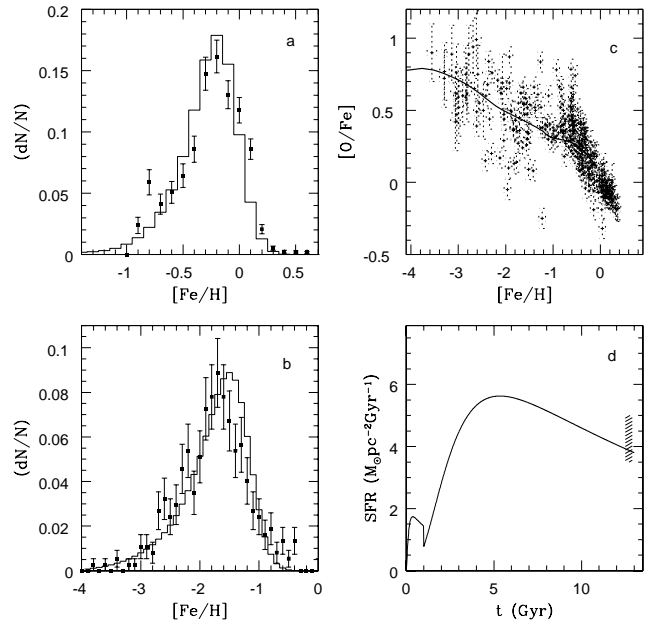


Figure 1. Comparison between the results of MW model (solid lines) and observations of a) the MDF in the MW at the solar neighbourhood (closed boxes with error-bars, Kotoneva et al. 2002), b) halo MDF at $R = R_\odot$ (Ryan & Norris 1991, closed boxes with statistical Poissonian error-bars), c) $[\text{O}/\text{Fe}]$ and $[\text{Fe}/\text{H}]$ for the stars observed at the solar neighbourhood (Carretta et al. 2000, who included reanalysis of Sneden et al. 1991, Tomkin et al. 1992, Kraft et al. 1992, Edvardsson et al. 1993; Gratton et al. 2003; Bensby, Feltzing & Lundström 2003; Cayrel et al. 2003), and d) the present-day SFR at the solar neighbourhood as summarised in Rana (1991, the shaded region).

Unfortunately, such observational estimates are not defined well enough to provide useful constraints on a chemical evolution model. Nevertheless, Fig. 1d demonstrates that our MW model is consistent with the broad range of the estimated SFR as summarised in Rana (1991).

Left panels of Fig. 2 show the predicted radial distribution of hydrogen column density (upper) and the oxygen (middle) and sulfur (bottom) abundances of the gas at the present-day, and compare them to the observations. The observed hydrogen surface density is obtained by summing the surface densities of H_2 and HI (Dame 1993)³. The result of our MW model is compatible with the observed hydrogen distribution at the inner radii within the uncertainties ($\approx 50\%$) of the observed values⁴. However, the hydrogen surface density at the outer radii is slightly overestimated when compared with the observations.

The predicted radial abundance profiles of oxygen and sulfur also reproduce the abundances observed in HII regions (Vilchez & Esteban 1996; Afferbach et al. 1997), although

³ The HI surface density profile has been recently confirmed by Nakanishi & Sofue (2003).

⁴ The contribution of HII should also be considered. However, so far no reliable measurement has been achieved, since it is not straightforward.

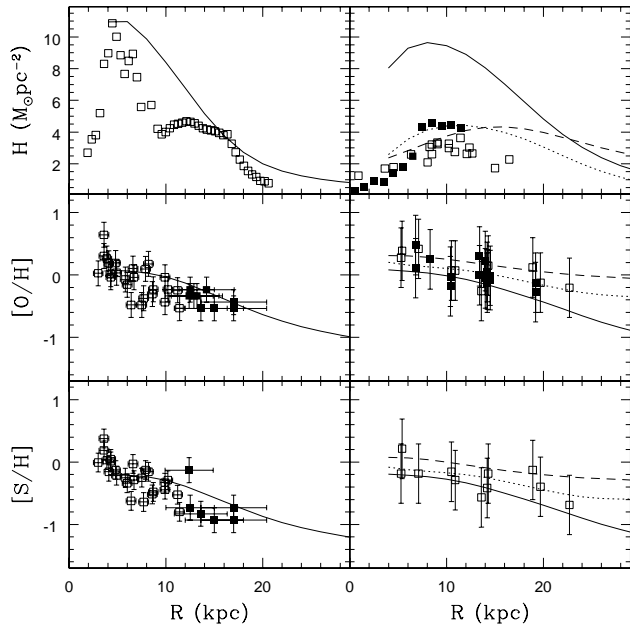


Figure 2. Radial distributions of the hydrogen surface density (upper) and of the oxygen (middle) and sulfur (bottom) abundances at the present-day for the MW model (left) and the M31 models (right). In the left panels, the solid lines are for the MW model results. In the right panels, solid, dotted and dashed lines display the M31a, M31b and M31c models, respectively. The observed distributions of the total surface density of hydrogen for the MW are from Dame (1993, open boxes), and those for M31 are from Dame et al. (1993, open boxes) and Loinard et al. (1999, closed boxes). Observations of abundances in HII regions in the MW from Vilchez & Esteban (1996) and Afflerbach et al. (1997) (closed and open boxes, respectively) are shown in the left panels. Those in M31 from Dennefeld & Kunth (1981) and Blair et al. (1982) (closed and open boxes, respectively) are shown in the right panels.

at the outer radii the model slightly overestimates the sulfur abundances.

Our semi-analytic model, whose parameter values summarised in Table 1, satisfies the general MW observational constraints. We now use the same framework to study the chemical evolution of M31.

4 THE M31 MODELS

The M31 models employ for the disc a different surface density profile from that of the MW model. Since the halo density profile of M31 is unknown, we adopt the same halo profile used in the MW model (see Section 2.2). The SF history of halo and disc is described by the parameters listed in Table 1. In Section 4.1, we first show a M31 model which adopts the same parameter set of our MW model. This model fails to reproduce some crucial features observed in M31. Therefore, in Sections 4.2 and 4.3, we present two models able to better explain the key observations.

4.1 M31a model: MW analogue

First, we construct a M31 model (M31a) with the same parameter values of our MW model. These parameters are summarised in Table 1. The right panels of Fig. 2 show the radial distributions of the hydrogen surface density and the radial profiles of the oxygen and sulfur abundances of the gas phase. The radial profiles of oxygen and sulfur abundances are reproduced within the observational errors. The M31a model results in too high hydrogen surface density when compared with the data. This is because the observed hydrogen surface density in M31 is smaller than in the MW.

Fig. 3 shows the radial profile for the mean $\langle[\text{Fe}/\text{H}]\rangle$ ($\langle[\text{Fe}/\text{H}]\rangle$) of main-sequence (MS) stars for the M31a model. Hereafter we simply call $\langle[\text{Fe}/\text{H}]\rangle$ the "mean metallicity". Model results are compared with observations by Bellazzini et al. (2003)⁵. We have chosen as reference fields those which are mostly disc- (or halo-) dominated, with estimated halo- (or disc-) contamination around or lower than 10% (see Table 1 in Bellazzini et al. 2003): the disc-dominated fields (G287, G119, G33, G76, G322 and G272) lie at deprojected⁶ galactocentric distances $R \approx 8$ kpc, $R \approx 12$ kpc, $R \approx 13$ kpc, $R \approx 14$ kpc, $R \approx 15$ kpc and $R \approx 18$ kpc, respectively; the halo-dominated fields (G319, G11, G351, G219 and G1) lie at projected galactocentric distances $R \approx 16$ kpc, $R \approx 17$ kpc, $R \approx 19$ kpc, $R \approx 20$ kpc and $R \approx 34$ kpc, respectively. Fig. 3 shows that M31a is in broad agreement with the observed mean metallicity in the disc-dominated fields, though the metallicity gradient is slightly steeper than the observed one (Table 2). On the other hand, the mean metallicity of the halo in M31a is too low, compared to the data.

To overcome the failure of M31a, we explored the parameter space of the M31 models which could explain the observational properties of M31, and found two viable solutions. In the following, we present these two models.

4.2 M31b model: our best model

The model parameters of M31b are summarised in Table 1. Compared with the M31a model, i.e. the MW analogue, this model has a shorter time-scale for the infall of disc gas (i.e. smaller a_d and b_d) and higher disc and halo SFE. We found that a combination of higher disc SFE and shorter time-scale for the disc infall leads to better agreement with the observed radial profile of the hydrogen surface density. In addition, a higher SFE in the halo phase leads to a more metal-rich halo, and we adopt a SFE 100 times higher in the halo phase than the M31a model.

In M31b the radial profile of the oxygen and sulfur abundances reproduces the observational data to roughly the same degree of the M31a model (Fig. 2). On the other hand, the higher disc SFE leads to stronger SF and therefore larger depletion of gas, and lower present-day hydrogen surface density than in M31a. Consequently, the result of

⁵ The observed MDFs are derived from red giant branch (RGB) stars, whereas the model produces the MDFs of MS stars, since it is difficult to construct MDFs of RGB stars within our framework. We assume that this inconsistency does not affect our comparison significantly.

⁶ The inclination angle of the M31 disc is $i_{\text{M31}} \approx 12.5^\circ$.

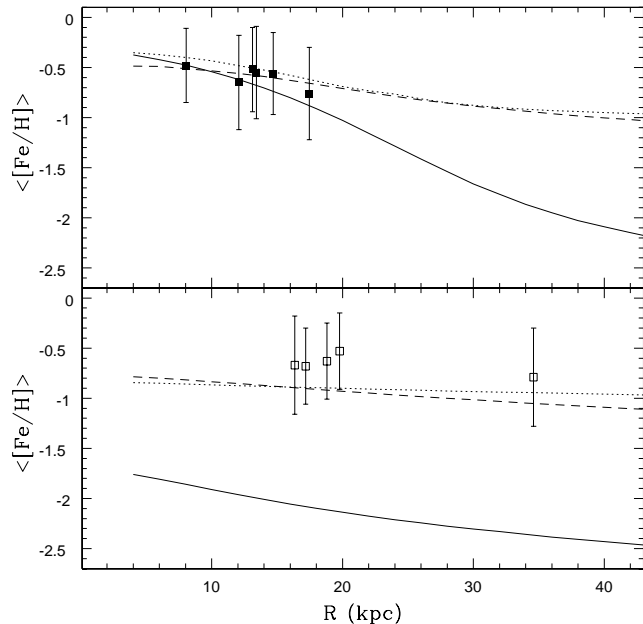


Figure 3. Present-day radial profile of the mean stellar metallicity of both disc (upper panel) and halo (lower panel). Solid, dotted and dashed lines represent the results of the M31a, M31b and M31c models, respectively. The mean metallicities from Bellazzini et al. (2003) are also shown (closed boxes with 1σ dispersion of their MDF).

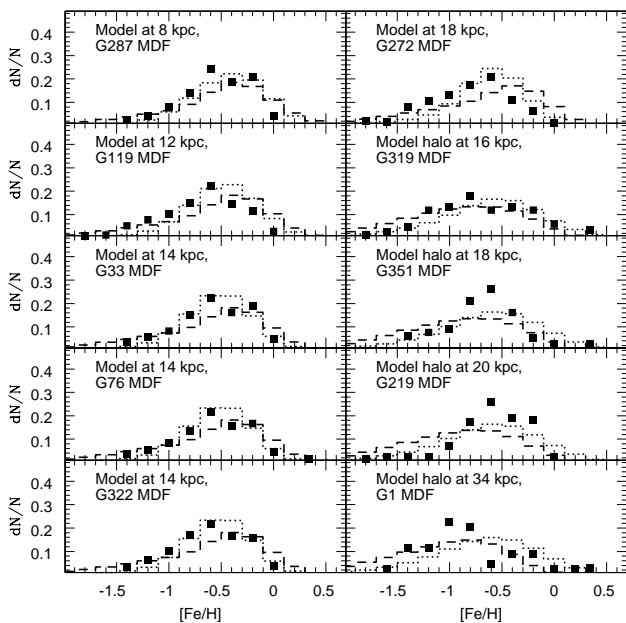


Figure 4. The MDFs of the M31b and M31c models (dotted and dashed lines, respectively). The MDFs observed from Bellazzini et al. (2003) are also shown (closed boxes).

the M31b model is in better agreement with the observed radial profile of the hydrogen surface density (Fig. 2). The hydrogen surface density profiles in both the M31b model and the observations peak at a radius of ≈ 8 kpc with a value of $\approx 4.5 M_{\odot} \text{pc}^{-2}$ (Loiarnard et al. 1999). However, like in the MW model, the hydrogen surface density at the outer radii is overestimated in M31b when compared with observations from Dame et al. (1993). We have tried to reproduce the observed hydrogen surface density at the outer radii by changing various parameters, however, we are unable to find a better parameter set than the M31b model. This might suggest that, to explain the low gas surface density at the outer radii in M31, another mechanism which is not included in our semi-analytic model is required.

The additional benefit of the shorter time-scale of the disc infall in M31b is its smaller SFR at the present-day. Since M31b has a SFR which peaks at an earlier epoch than M31a, M31b predicts a lower present-day SFR ($\approx 1.5 M_{\odot} \text{yr}^{-1}$) in the disc (4 - 20 kpc) than M31a ($\approx 2.4 M_{\odot} \text{yr}^{-1}$). The observational estimates of the present-day SFR in M31 still have a large uncertainty. For example, Williams (2002) estimated the SFR for the last ≈ 5 Gyr between roughly 2 and $20 M_{\odot} \text{yr}^{-1}$, while Williams (2003) inferred that the total SFR for the M31 disc has been $\approx 1 M_{\odot} \text{yr}^{-1}$ over the past 60 Myr. This value is higher than the SFR of $\approx 0.2 M_{\odot} \text{yr}^{-1}$ estimated from H α and Far Infra-Red luminosities (Devereux et al. 1994). In addition, all these values could be affected by systematic errors (e.g. Bell 2003). Nevertheless, these observations suggest that M31 has a lower SFR than the MW, and M31b is consistent with this trend.

Fig. 3 shows improved agreement between the results of the M31b model and the observations of the mean metallicity for both disc- and halo-dominated fields. In the disc, M31b has a shallower metallicity gradient than M31a, and better reproduces the observed gradient (Table 2). This is mainly due to the small b_d we adopted (Table 1).

Fig. 4 directly compares the MDFs of M31b with the MDF obtained in Bellazzini et al. (2003) in different fields. The model MDFs are derived from main-sequence stars, and convolved with a Gaussian error function with $\sigma = 0.25$ dex. There is qualitative agreement between the MDFs of the M31b model and those observed, especially in the disc-dominated fields. The main exception is the G1 halo-dominated field, whose observed MDF is more metal-poor and bimodal. The MDFs of the G351 and G219 halo-dominated fields show narrower peaks than those of the model. Differences in the shape of the observed halo MDFs among the different fields suggest possible inhomogeneities in the M31 halo (see also Bellazzini et al. 2003).

In the framework of our semi-analytic models, M31b gives the best fit for the observational constraints available in M31. In Section 5, we discuss the formation process of M31 which is implied by these results.

4.3 M31c model: another possible model

The result of the M31b model suggests that a stronger halo SF can produce a metal-rich halo. However, applying the higher SFE is not the only way to induce stronger SF. This can also be achieved by employing a larger reservoir of infalling halo gas, without increasing the SFE. Here we discuss

Table 2. Radial gradients for the mean stellar metallicity of the MDFs in the M31 models. The results for the MW model and for the fields observed in Bellazzini et al. (2003) are also presented as reference.

	$(\Delta\langle[Fe/H]\rangle/\Delta R)^a$	$(\Delta\langle[Fe/H]\rangle/\Delta R)^b$
MW	-0.058	-0.021
M31 _{obs}	-0.026	-0.008
M31a	-0.041	-0.021
M31b	-0.021	-0.003
M31c	-0.014	-0.009

^a This value (dex/kpc) refers to the range 4 - 16 kpc for the MW model and 4 - 20 kpc for the M31 models.

^b This value (dex/kpc) refers to the range 4 - 30 kpc in the halo of the MW and M31 models.

the M31c model, which assumes a much larger present-day halo surface density and a longer (6 Gyr) halo phase (Table 1). Again, to explain the observed hydrogen surface density, M31c uses a shorter disc infall time-scale, and a weaker radial dependence, which also leads to a present-day SFR similar to M31b.

Fig. 2. shows the predicted radial distributions of oxygen and sulfur abundances which are in agreement with the observational data to roughly the same degree of the other models. The hydrogen surface density profile of the M31c model is consistent with Dame et al. (1993) in the inner region of the disc, $R < 12$ kpc. However, M31c has a broader peak at a larger radius than M31b. Consequently, the model overestimates the surface density in the outer region, $R > 12$ kpc. Again, this result might suggest that additional physical mechanisms operate, to explain the observed low hydrogen surface density at the outer radii.

Fig. 3 shows that M31c also reproduces the observed radial distributions of the metallicity, similarly to M31b. The metallicity gradient in M31c is flatter than M31b at the inner radii as a consequence of the weaker radial dependence of the disc infall time-scale (i.e. a smaller b_d). In the halo fields, M31c also has systematically higher metallicity than M31a and a steeper gradient than M31b. Although the gradient is in better agreement with the observations than M31b (Table 2), M31c has lower mean metallicities than observed, especially at the outer radii. In Fig. 4, the predicted MDFs at different radii are displayed. The MDFs of M31c are also in good agreement with those observed, especially in the disc. On the other hand, the halo MDFs show a more pronounced metal-poor tail than in M31b.

Thus, the M31c model also leads to acceptable results, although M31b is in better agreement with the observations. The next section discusses the formation history of M31 implied by the M31b and M31c models.

5 DISCUSSION

The results in the previous section have shown that the main trends of the chemical evolution history of both the MW and M31 can be described using the same framework. We have also found that to explain the observations in more detail, different sets of parameter values for the formation

history are required for the MW and M31, respectively. In this section, we discuss how these different parameters values relate to different galaxy formation histories.

The previous sections have shown that the main differences between the MW and M31 include the hydrogen surface density in the disc and, more significantly, the halo metallicity. The smaller hydrogen surface density in M31 can be explained by a combination of the shorter disc infall time-scale and the higher disc SFE.

The most striking difference is that the mean metallicity observed in the M31 halo is about ten times higher than that observed in the MW halo, though both galaxies have similar mass and morphology. *Which is a “typical” halo?* Metal-rich halos seem more common than metal-poor ones, as pointed out by Zibetti et al. (2004) who analysed a sample of about 1000 edge-on disc galaxies within the SDSS. Harris & Harris (2001) have also shown that the NGC5128 halo MDF closely resembles that in the M31 halo. This similarity is perhaps suggestive of a common history in the halo formation of both galaxies, despite their different Hubble-type.

A straightforward way to obtain a more metal-rich halo would be by requiring homogeneous pre-enrichment of the infalling halo gas with a metallicity $Z \approx 0.1 Z_\odot$. However, this metallicity seems too high, if such pre-enrichment occurred homogeneously in the whole universe. For example, although this value is close to the mean metallicity of Damped Lyman α systems (DLAs), many DLAs have much lower metallicity (Pettini 2003; Prochaska et al. 2003). If DLAs are more evolved systems than the infalling halo gas, their metallicity should be higher than that induced by pre-enrichment. Therefore, a pre-enrichment of $Z \approx 0.1 Z_\odot$ may not be tenable.

We found that the observed metal-rich halo of M31 could be explained by two scenarios without any pre-enrichment: a) a higher halo SFE; b) a larger reservoir of infalling halo gas with a longer halo phase. Scenario a) might be explained in a hierarchical clustering regime, where the halo is formed by accretion of building-blocks. Theory predicts that gas removal by supernova-driven winds should be more effective in lower mass systems, leading to a consequent suppression of the SFR and a low SFE (e.g. Dekel & Silk 1986; Efsthathiou 2000). In addition, observations based on the SDSS also suggest that the SFE decreases with decreasing stellar mass in low mass galaxies with a stellar mass $M_\star < 3 \times 10^{10} M_\odot$ (Kauffmann et al. 2003). Therefore, higher SFE in the M31 halo phase would be explained if the building-blocks of the M31 halo are systematically higher mass systems than those of the MW halo (see also Harris & Harris 2001). This result again supports the notion of diversity in the formation of spiral galaxies which are apparently similar in mass and morphology and belong to the same Local Group. Admittedly, our model does not adhere to the hierarchical-clustering scenario in a self-consistent manner, however, our chemical evolution models can be interpreted as the “mean” SF and chemical evolution history of the stars which end up at each radius.

As an observational consequence of our models, we found that both scenarios a) and b) predict a more massive stellar halo in M31, respectively about 6 and 9 times more massive than in the MW, whose stellar halo mass is $\approx 10^9 M_\odot$. This result suggests that there might be a correlation between the halo metallicity and its stellar mass.

Using dynamical simulations, Bekki, Harris & Harris (2003) show that the stellar halo comes from the outer part of the progenitor discs when the bulge is formed by a major merger of two spiral galaxies. Based on this, they also predict the correlation of the metallicity of the stellar halos and the mass of the bulges which were formed by major mergers, since larger bulges have the larger progenitors, and progenitor spiral galaxies should follow the observed mass-metallicity relation. Although they do not mention a correlation between the masses of the bulge and halo, it would naturally be expected. Thus, a major merger scenario could explain our conclusion. Future observational surveys will better quantify the correlation between the halo metallicity and its stellar mass (e.g. Mouhcine et al. 2003).

It is possible to distinguish scenarios a) and b) through observation. First, due to a longer halo phase, scenario b) predicts intermediate-age population in the M31 halo. This picture could explain the recent evidence of intermediate-age population by deep imaging of the M31 halo (Brown et al. 2003).

It is worth mentioning that the metallicity gradient in the stellar halo is sensitive to the assumed stellar halo density profile especially in scenario b); a steeper density profile leads to a steeper metallicity gradient. Pritchett & van den Bergh (1994) suggested that the outer halo of M31 can be modeled by a power law surface brightness profile of $I \propto R^{-4}$, which is much steeper than what we assumed ($\propto R^{-2}$). We found that such a steep profile rules out scenario b) to reproduce the flat metallicity gradient observed in the M31 halo. However, it is still difficult to accurately measure the halo surface brightness of M31 (e.g. Zibetti et al. 2004). Thus, more observational estimates of the M31 halo surface brightness profile would be an important test for this scenario.

We also found that the higher halo SFE in scenario a) leads to about 0.2 dex higher [O/Fe] when [Fe/H] < -1 dex, due to intense halo SF. Although measuring [O/Fe] is a hard challenge for the current available instruments, this task could be accomplished by the next-generation large-aperture optical telescope.

5.1 Prospect

The framework we have used can explain the main trends in the chemical properties of both the MW and M31. However, recent observations of stellar streams both in the MW (e.g. Helmi et al. 1999; Chiba & Beers 2000; Ibata et al. 2002; Brook et al. 2003; Navarro, Helmi & Freeman 2004; Majewski et al. 2004) and M31 (Ibata et al. 2001; McConnachie et al. 2003; Merrett et al. 2003; Zucker et al. 2004; Lewis et al. 2004) clearly identify inhomogeneities in the chemical and dynamical history of both galaxies, which could suggest that a significant fraction of the halo stars results from later accretion of satellite galaxies. In the light of these recent observations, it will be important to study both the MW and M31 in more detail by employing a self-consistent chemo-dynamical model (e.g. Brook et al. 2004) to trace their interrelated chemical and dynamical histories.

ACKNOWLEDGMENTS

We thank the anonymous referee for comments which much improved this manuscript. We acknowledge the financial support of the Australian Research Council through its Discovery Project scheme.

REFERENCES

- Afflerbach A., Churchwell E., Werner M.W., 1997, *ApJ*, 478, 190
 Alibés A., Labay J., Canal R., 2001, *A&A*, 370, 1103
 Asplund A., in “Elemental Abundances in Old Stars and Damped Lyman α Systems”, 25th meeting of the IAU, Joint Discussion 15, 2003, Sydney, Australia
 Bekki K., Chiba M., 2001, *ApJ*, 558, 666
 Bekki K., Harris W.E., Harris G.L.H., 2003, *MNRAS*, 338, 587
 Bell E.F., 2003, *ApJ*, 586, 794
 Bellazzini M., Cacciari C., Federici L., Fusi Pecci F., Rich M., 2003, *A&A*, 405, 867
 Bensby T., Feltzing S., Lundström L., 2004, *A&A*, 415, 155
 Bertelli G., Nasi E., 2001, *AJ*, 121, 1013
 Binney J., Tremaine S., *Galactic dynamics*, 1987, Princeton University Press, Princeton
 Blair W.P., Kirshner R.P., Chevalier R.A., 1982, *ApJ*, 254, 50
 Brook C.B., Kawata D., Gibson B.K., Flynn C., 2003, *ApJ*, 585, L125
 Brook C.B., Kawata D., Gibson B.K., Flynn C., 2004, *MNRAS*, 349, 52
 Brown T.M., Ferguson H.C., Smith E., Kimble R.A., Sweigart A.V. et al., 2003, *ApJ*, 592, L17
 Carretta E., Gratton R.G., Sneden C., 2000, *A&A*, 356, 238
 Cayrel R., Depagne E., Spite M., Hill V., Spite F. et al., 2004, *A&A*, 416, 1117
 Chang R.X., Hou J.L., Shu C.G., Fu C.Q., 1999, *A&A*, 350, 38
 Chiappini C., Matteucci F., Gratton R., 1997, *ApJ*, 477, 765
 Chiba M., Beers T.C., 2000, *AJ*, 119, 2843
 Chiba M., Beers T.C., 2001, *ApJ*, 549, 325
 Cowie L., Songaila A., 1998, *Nature*, 394, 44
 Dame T.M., 1993, in Holt S.S., Verter F. eds, “Back to the Galaxy”, AIP Conf. 278, p. 267
 Dame T.M., Koper E., Israel F.P., Thaddeus P., 1993, *ApJ*, 418, 730
 Dekel A., Silk J., 1986, *ApJ*, 303, 39
 Dennefeld M., Kunth D., 1981, *AJ*, 86, 989
 Devereux N.A., Price R., Wells L.A., Duric N., 1994, *AJ*, 108, 1667
 Diaz A.I., Tosi M., 1984, *MNRAS*, 208, 365
 Durrell P.R., Harris W.E., Pritchett C.J., 2001, *AJ*, 121, 2557
 Edvardsson B., Andersen J., Gustafsson B., Lambert D.L., Nissen P.E. et al., 1993, *A&A*, 275, 101
 Efstathiou G., 2000, *MNRAS*, 317, 697
 Eggen O.J., Lynden-Bell D., Sandage A.R., 1962, *ApJ*, 136, 748
 Fenner Y., Gibson B.K., 2003, *PASA*, 20, 189

- Ferguson A.M.N., Johnson R.A., 2001, *ApJ*, 559, L13
- Ferguson A.M.N., Irwin M.J., Ibata R.A., Lewis G.F., Tanvir N.R., 2002, *AJ*, 124, 1452
- Freeman K.C., 1999, in Gibson B.K., Axelrod T.S., Putman M.E. eds, "The Third Stromlo Symposium: The Galactic Halo", ASP Conference Series, Vol. 165, p. 167
- Freeman K., Bland-Hawthorn J., 2002, *ARA&A*, 40, 487
- Freudenreich H.T. 1998, *ApJ*, 492, 495
- Gibson B.K., Fenner Y., Renda A., Kawata D., Lee H.-c., 2003, *PASA*, 20, 401
- Goswami A., Prantzos N., 2000, *A&A*, 359, 191
- Gratton R.G., Carretta E., Claudi R., Lucatello S., Barbieri M., 2003, *A&A*, 404, 187
- Greggio L., Renzini A., 1983, *A&A*, 118, 217
- Harris W.E., Harris G.L.H., 2001, *AJ*, 122, 3065
- Helmi A., White S.D.M., de Zeeuw P.T., Zhao, H., 1999, *Nature*, 402, 53
- Hernandez X., Valls-Gabaud D., Gilmore G., 2000, *MNRAS*, 316, 605
- Holland S., Fahlman G.G., Richer H.B., 1996, *AJ*, 112, 1035
- Ibata R.A., Irwin M.J., Lewis G.F., Ferguson A.M.N., Tanvir N.R., 2001, *Nature*, 412, 49
- Ibata R.A., Lewis G.F., Irwin M.J., Cambr esy L., 2002, *MNRAS*, 332, 921
- Iwamoto K., Brachwitz F., Nomoto K., Kishimoto N., Umeda H. et al., 1999, *ApJS*, 125, 439
- Kauffmann G., Heckman T.M., White S.D.M., Charlot S., Tremonti C. et al., 2003, *MNRAS*, 341, 54
- Kennicutt R.C. Jr., 1998, *ARA&A*, 36, 189
- Kotoneva E., Flynn C., Chiappini C., Matteucci F., 2002, *MNRAS*, 336, 879
- Kraft R.P., Sneden C., Langer G.E., Prosser C.F., 1992, *AJ*, 104, 645
- Kroupa P., Tout C.A., Gilmore G., 1993, *MNRAS*, 262, 545
- Kuijken K., Gilmore G., 1991, *ApJ*, 367, L9
- Lewis G.F., Ibata R.A., Chapman S.C., Ferguson A.M.N., McConnachie A.W. et al., in Gibson B.K., Kawata D. eds, *Proceedings of Galactic ChemoDynamics V*, to appear on *PASA*
- Loinard L., Dame T.M., Heyer M.H., Lequeux J., Thaddeus P., 1999, *A&A*, 351, 1087
- Majewski S.R., Kunkel W.E., Law D.R., Patterson R.J., Polak A.A. et al., 2004, *AJ*, 128, 245
- Matteucci F., Franois P., 1989, *MNRAS*, 239, 885
- McConnachie A.W., Irwin M.J., Ibata R.A., Ferguson A.M.N., Lewis G.F. et al., 2003, *MNRAS*, 343, 1335
- Merrett H.R., Kuijken K., Merrifield M.R., Romanowsky A.J., Douglas N.G. et al., 2003, *MNRAS*, 346, L62
- Moll a M., Ferrini F., Diaz A.I., 1996, *ApJ*, 466, 668
- Mouhcine M., Ferguson H.C., Rich R.M., Brown T., Smith E., 2003, in Combes F., Barret D., and Contini T. eds, "Semaine de l'Astrophysique Franaise", Bordeaux, EDP Sciences, Conference Series, p. 122.
- Nakanishi H., Sofue Y., 2003, *PASJ*, 55, 191
- Navarro J.F., Helmi A., Freeman K.C., 2004, *ApJ*, 601, 43
- Pagel B.E.J., Tautvaišiene G., 1995, *MNRAS*, 276, 505
- Pettini M., lectures given at the XIII Canary Islands Winter School of Astrophysics, 'Cosmochemistry: The Melting Pot of Elements', Cambridge University Press
- Preston G.W., Shectman S.A., Beers T.C., 1991, *ApJ*, 375, 121
- Pritchett, C.J., van den Bergh, S., 1994, *AJ*, 107, 1730
- Prochaska J.X., Gawiser E., Wolfe A.M., Castro, S., Djorgovski, S.G., 2003, *ApJ*, 595, L9
- Putman M.E., Bland-Hawthorn J., Veilleux S., Gibson B.K., Freeman K.C. et al., 2003, *ApJ*, 597, 948
- Rana, N.C., 1991, *ARA&A*, 29, 129
- Reitzel D.B., Guhathakurta P., 2002, *AJ*, 124, 234
- Reitzel D.B., Guhathakurta P., Rich R.M., 2004, *AJ*, 127, 2133
- Renzini A., Voli M., 1981, *A&A*, 94, 175
- Rich R.M., Reitzel D.B., Guhathakurta P., Gebhardt K., Ho L.C., 2004, *AJ*, 127, 2139
- Robin A.C., Creze M., Mohan V., 1992, *ApJ*, 400, L25
- Ruphy S., Robin A.C., Epchtein N., Copet E., Bertin E. et al., 1996, *A&A*, 313, L21
- Ryan S.G., Norris J.E., 1991, *AJ*, 101, 1865
- Sakamoto T., Chiba M., Beers T.C. 2003, *A&A*, 397, 899
- Sarajedini A., van Duyne J., 2001, *AJ*, 122, 2444
- Schaller G., Schaerer D., Meynet G., Maeder A., 1992, *A&AS*, 96, 269
- Searle L., Zinn R., 1978, *ApJ*, 225, 357
- Sembach K.R., Gibson B.K., Fenner Y., Putman M.E., 2002, *ApJ*, 572, 178
- Sneden C., Kraft R.P., Prosser C.F., Langer G.E., 1991, *AJ*, 102, 2001
- Talbot R.J. Jr., Arnett W.D., 1971, *ApJ*, 170, 409
- Thilker D.A., Braun R., Walterbos R.A.M., Corbelli E., Lockman F.J. et al., 2004, *ApJ*, 601, L39
- Timmes F.X., Woosley S.E., Weaver T.A., 1995, *ApJS*, 98, 617
- Tinsley B.M., 1980, *Fund. Cosm. Phys.*, 5, 287
- Tomkin J., Lemke M., Lambert D.L., Sneden C., 1992, *AJ*, 104, 1568
- van den Bergh S., in "The Local Group as an Astrophysical Laboratory", Cambridge University Press 2003
- Vilchez J.M., Esteban C., 1996, *MNRAS*, 280, 720
- Walterbos R.A.M., Kennicutt R.C. Jr., 1988, *A&A*, 198, 61
- Williams B.F., 2002, *MNRAS*, 331, 293
- Williams B.F., 2003, *AJ*, 126, 1312
- Woosley S.E., Weaver T.A., 1995, *ApJS*, 101, 181
- Worthey G., Espa a A.L., 2003, in McWilliam A., Rauch M. eds, *Carnegie Observatories Astrophysics Series, Vol. 4: "Origin and Evolution of the Elements"*, (Pasadena: Carnegie Observatories, <http://www.ociw.edu/ociw/symposia/series/symposium4/proceedings.html>)
- Wyse R.F.G., Silk J., 1989, *ApJ*, 339, 700
- Zibetti S., White S.D.M., Brinkmann J., 2004, *MNRAS*, 347, 556
- Zucker D.B., Kniazev A.Y., Bell E.F., Martinez-Delgado D., Grebel E.K. et al., 2004, *ApJ*, 612, L117

This paper has been typeset from a \TeX / \LaTeX file prepared by the author.